Distinguishing prompt-collapse binary neutron star mergers from binary black holes: Tidal effects and remnant properties

Arnab Dhani,[1,2,3,*] Alessandro Camilletti,[4,5,6] David Radice,[2,3,7,†] Rahul Kashyap,[8,2,3] Bangalore Sathyaprakash,[2,3,9] Domenico Logoteta,[10,11] and Albino Perego[4,5]

[1]*Max Planck Institute for Gravitational Physics (Albert Einstein Institute), Am Mühlenberg 1, Potsdam 14476, Germany*
[2]*Institute for Gravitation and the Cosmos, The Pennsylvania State University, University Park, Pennsylvania 16802, USA*
[3]*Department of Physics, The Pennsylvania State University, University Park, Pennsylvania 16802, USA*
[4]*Dipartimento di Fisica, Università di Trento, Via Sommarive 14, 38123 Trento, Italy*
[5]*INFN-TIFPA, Trento Institute for Fundamental Physics and Applications, Via Sommarive 14, I-38123 Trento, Italy*
[6]*Data Science for Industry and Physics, Fondazione Bruno Kessler, via Sommarive 18, 38123, Trento (TN), Italy*
[7]*Department of Astronomy and Astrophysics, The Pennsylvania State University, University Park, Pennsylvania 16802, USA*
[8]*Department of Physics, Indian Institute of Technology Bombay, Mumbai 400076, India*
[9]*School of Physics and Astronomy, Cardiff University, Cardiff, UK, CF24 3AA*
[10]*Dipartimento di Fisica, Università di Pisa, Largo B. Pontecorvo, 3 I-56127 Pisa, Italy*
[11]*INFN, Sezione di Pisa, Largo B. Pontecorvo, 3 I-56127 Pisa, Italy*

(Received 3 August 2025; accepted 27 October 2025; published 1 December 2025)

We study the properties of remnants formed in prompt-collapse binary neutron star mergers. We consider nonspinning neutron star binaries over a range of total masses and mass ratios across a set of 22 equations of state, totaling 107 numerical relativity simulations. We report the final mass and spin of the systems (including the accretion disk and ejecta) to be constrained in a narrow range—$0.98 \lesssim M_f/M \lesssim 0.99$ for the mass and $0.85 \lesssim a_f \lesssim 0.95$ for the dimensionless spin—regardless of the binary configuration and matter effects. This sets them apart from binary black hole merger remnants. We assess the detectability of the postmerger signal in a future 40 km Cosmic Explorer observatory and find that the signal-to-noise ratio in the postmerger of an optimally located and oriented binary at a distance of 100 Mpc can range from < 1 to 8, depending on the binary configuration and equation of state, with a majority of them greater than 4 in the set of simulations that we consider. We also consider the distinguishability between prompt-collapse binary neutron star and binary black hole mergers with the same masses and spins. We find that Cosmic Explorer will be able to distinguish such systems primarily via the measurement of tidal effects in the late inspiral. Neutron star binaries with *reduced tidal deformability* $\tilde{\Lambda}$ as small as ~ 3.5 can be identified up to a distance of 100 Mpc, while neutron star binaries with $\tilde{\Lambda} \sim 22$ can be identified to distances greater than 250 Mpc. This is larger than the distance up to which the postmerger will be visible. Finally, we discuss the possible implications of our findings for the equation of state of neutron stars from the gravitational wave event GW230529.

DOI: 10.1103/2yng-9l9s

I. INTRODUCTION

The observations of gravitational waves (GWs) from compact binary mergers [1,2] have informed us of the astrophysical population of such sources, allowed for precision tests of strong-field gravity [3,4], provided an independent measurement of the expansionary history of the Universe [5,6], and offered a tantalizing prospect of inferring the neutron star (NS) equation of state (EoS) [7]. With improving sensitivities of ground-based

*Contact author: arnab.dhani@aei.mpg.de
†Alfred P. Sloan fellow.

detectors [8–10] and the ongoing planning for future observatories [11–13], the precision with which we can measure source properties [14–16] and infer the nature of gravity in the strong-field regime and on large scales will improve many fold. Specifically, the proposed next-generation of ground-based gravitational wave detectors, such as Cosmic Explorer (CE) [11] and Einstein Telescope [17], can observe $O(\text{few}M_\odot)$ compact binary mergers up to a redshift of $z \sim 1$ [14] and measure the radius of NS at a precision of a few tens to 100 m [16,18–23].

This population of sources can be comprised of binary neutron stars (BNSs), binary black holes (BBHs), or neutron star - black holes. It is imperative that one has an unbiased inference of the source class and its characteristics. For instance, LIGO-Virgo-KAGRA (LVK) observations alone cannot rule out the possibility that GW170817 [24], the first BNS merger observed by LVK Collaboration, and GW190425 [25] are low-mass BBH mergers [7]. In the case of GW170817, it was the subsequent detection of short gamma ray burst and kilonova [26] that conclusively classified the event as an NS merger. The absence of an electromagnetic (EM) counterpart for GW190425 means that the event is classified as a BNS merger only because of its component masses [25]. However, under the assumption that the event was a BNS merger, there is a 96%–97% probability that the remnant promptly collapsed to a black hole (BH) [25]. An accurate source classification is of immense value for both astrophysical and fundamental physics inferences. First, one of the most important observables of interest in nuclear physics is the maximum mass of NSs, because it depends on the EoS at extreme densities and reveals the potential for NS cores to host hyperons or quarks [27]. Second, one of the widely used methods to test the nature of strong gravity and the dynamics of black hole binaries is the *inspiral-merger-ringdown* consistency test [28,29]. Therefore, an incorrect identification of a BNS merger as a BBH merger can lead to a false violation of general relativity [30].

The outcome of a BNS merger can be one of the following: a stable differentially rotating NS, an unstable short-lived NS undergoing a delayed collapse due to the inability of the differential rotation to support the remnant mass on a secular timescale, or a prompt collapse to a BH on a dynamical timescale. The radiated energy and angular momentum of the system depend on the nature of the formed remnant. Long-lived NS remnants are efficient emitters of GWs, while, in a prompt collapse, the remnant—including the disk and ejecta—is expected to retain most of the mass and angular momentum of the system, even though the peak luminosity is greater in the latter case [31]. The delineation of a prompt collapse and a remnant NS is given by the threshold mass M_{thres}, which is defined as the minimum total mass of a binary that leads to a prompt collapse [32] and depends weakly on its mass ratio for close to equal mass systems [32,33].

Prompt-collapse mergers have been widely studied with a focus on understanding the properties of the threshold mass [31–42] and its detectability [36], since its determination can inform the maximum mass and compactness supported by the EoS of NSs. This is because it is currently unknown whether core-collapse supernovae, expected to be the primary formation mechanism of NS in binaries, can produce NSs across the entire mass range supported by a given EoS, since most galactic NSs lie between 1.3 and $1.4M_\odot$ [43]. However, the properties of the remnants, their astrophysical significance, and the detectability of a generic prompt collapse from GW observations with future detectors have only recently started getting attention [41,42,44–46].

In the absence of an EM counterpart, BNS mergers are distinguished from BBH mergers by the presence of tidal interactions between the NSs. However, heavier NSs are more compact and have smaller tidal deformabilities. Therefore, even if such heavy NSs are produced astrophysically and form binaries, it is currently unknown whether future detectors can measure their tidal deformabilities with sufficient accuracy to confidently classify them as a BNS merger. Consequently, it is currently not known what the maximum NS mass is that can be confidently measured using GW observations. These heavy binaries would also promptly collapse to a BH.

In this paper, we use data from 107 nonspinning BNS merger simulations, spanning 22 EoS and a wide range of masses and mass ratios, to investigate the properties of a GW signal from prompt-collapse BNS mergers. We find that the predicted remnant mass and spin (including the disk) are significantly greater than those produced by a corresponding BBH merger. Subsequently, we explore the detectability of the ringdown. We find that for a majority of systems, the ringdown can be observed up to a distance of 100 Mpc in a future observatory. Furthermore, we show the contrast in the signal power during the ringdown phase of prompt collapse and its BBH equivalent, as observed in a 40 km Cosmic Explorer detector, the former being more silent. Additionally, we ask and take the first steps toward answering the following dual question: what is the smallest tidal deformability that can be distinguished from zero using the inspiral phase of the system? Is it possible to distinguish between BNS and BBH mergers in the event that their inspiral signals are consistent with each other? We find that a future CE detector can distinguish virtually all BNS and BBH mergers up to a distance of 100 Mpc from the inspiral and a majority of these systems from their ringdowns too. At larger distances, the postmerger becomes very weak while the tidal deformabilities can still be well measured, depending on the stiffness of the EoS. Finally, we discuss the astrophysical consequences of identifying a prompt collapse with the progenitor of GW230529's primary component.

The rest of the paper is organized as follows. In Sec. II, we describe numerical relativity data used in this study.

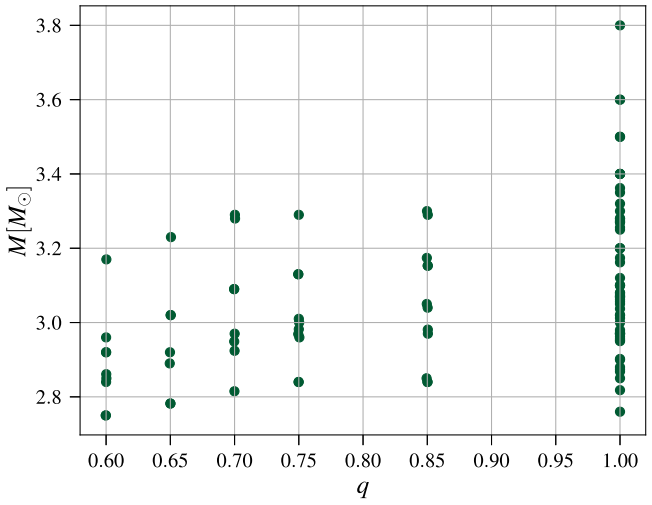

FIG. 1. The total mass of the binary at infinite separation and mass ratio of the 107 simulations used in this study.

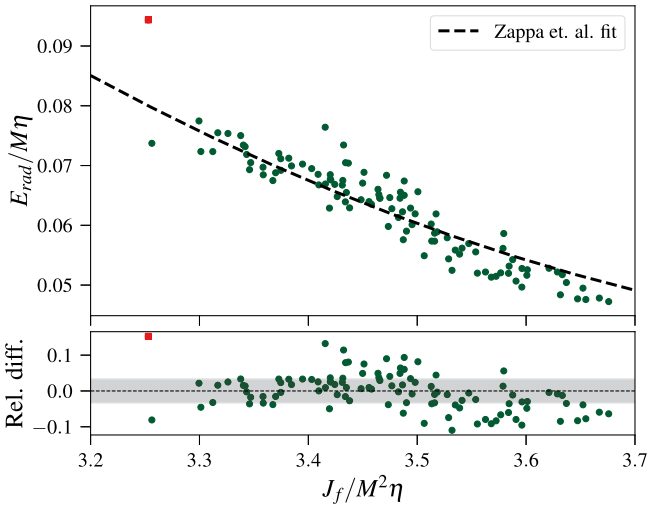

FIG. 2. Reduced total radiated energy versus reduced angular momentum of the remnant. The fit given in Zappa *et al.* [31] is overlayed in the top panel. The bottom panel shows the relative difference with respect to the fit, and the gray band shows the median of the absolute relative difference. The outlier denoted with a red square is the $1.7M_\odot - 1.7M_\odot$ system with the BA EoS (see the text for further discussion).

We report our results in Sec. III, where the remnant mass and spin of prompt-collapse remnants are compared to those of the corresponding BBH mergers. We evaluate their detectability and distinguishability compared to BBH merger ringdowns. We conclude in Sec. IV with a discussion of astrophysical implications and future work.

II. NUMERICAL RELATIVITY DATA

We consider 22 EoSs spanning a wide range in the corresponding nonrotating NS maximum masses and typical radii. In particular, we employ 15 finite-temperature EoSs: BHB$\Lambda\phi$ [47], BLh [48,49], DD2qG [50], HS (DD2) [51,52], LS220 [53], SFHo [54], SRO (SLy) [55,56], and nine variants of the SRO EoS with different values of the empirical nuclear parameters [56,57]. We also consider 6 zero-temperature β-equilibrated EoSs: ALF2 [58], H3 and H4 [59–61], the Big Apple EoS (BA from now on) [62], and the GRW1 and GRW2 EoSs [40]. The zero-temperature EoSs are supplemented with thermal effects using an adiabatic index, $\Gamma_{\rm th} = 1.7$, following, e.g., Refs. [32,63–65].

GRW1 and GRW2 are completely phenomenological EoSs, while the other models are nuclear theory based. Three EoSs include hyperons in addition to nucleons: BHB$\Lambda\phi$, H3, and H4. Three EoSs include a QCD phase transition to deconfined quarks: ALF2, BLQ, and DD2qG.

We consider a total of 107 numerical relativity simulations. The distribution of the total mass at infinite separation, M, and the mass ratio, q, considered in this study are shown in Fig. 1. These simulations have already been presented in Refs. [33,40], to which we refer for further details and to Ref. [66] for an up-to-date description of the simulation code capabilities. In brief, all simulations were initialized using quasicircular, irrotational binary initial data with the pseudospectral code Lorene [67] and evolved with the WhiskyTHC code [68–71]. The latter is built on top of the Einstein Toolkit [72] and makes use of the Carpet adaptive mesh refinement framework [73,74], which implements the Berger-Oliger scheme with refluxing [75,76]. As in these previous works, we classify as a prompt collapse those binaries for which the lapse function decreases monotonically below 0.2 until BH formation (no bounce).

III. RESULTS

A. Radiated energy and angular momentum

Energy and angular momentum are radiated during a compact binary merger in the form of gravitational waves, with the total radiated energy and angular momentum denoted by $E_{\rm rad}$ and $J_{\rm rad}$. The former is calculated from the Bondi News tensor, while the latter also uses the strain as input [77]. In practice, the Bondi News tensor is calculated by differentiating the strain. Zappa *et al.* [31] showed that the angular momentum of the merged remnant is uniquely determined by the total radiated energy. It was reported that this relationship holds regardless of the binary parameters, the EoS employed, or the microphysics incorporated in the simulations during the postmerger phase.

In Fig. 2, we plot the reduced radiated energy as a function of the reduced remnant angular momentum for the set of simulations used in this study. We also depict the quadratic fit given in Zappa *et al.* [31] for these quantities, with the bottom panel showing the residuals. We found that the coefficients of the fit reported in Zappa *et al.* [31] do not have sufficient significant digits required to reproduce the curve, and also contain a typographic error. The correct fit is given by [[78]],

$$e_{\rm rad} = c_2 j_{\rm rem}^2 + c_1 j_{\rm rem} + c_0, \tag{3.1}$$

where $e_{\rm rad} = E_{\rm rad}/(M\eta)$ and $j_{\rm rem} = J_f/(M^2\eta)$, η is the symmetric mass ratio, and J_f is the angular momentum of the remnant. The coefficients of the fit are $c_2 = 0.05334342$, $c_1 = -0.43994502$, and $c_0 = 0.94665103$. We find a median relative difference of ∼3.3% and a maximum of ∼15%. The observed agreement is nontrivial because very few simulations in the regime of $j_{\rm rem}$ explored in this paper—less than 10%—were originally present in Zappa *et al.* [31], and none of them resulted in a prompt collapse.

The binary with the largest deviation—residing at 3σ in the residual distribution and marked by a red square—in Fig. 2 is the $1.7M_\odot - 1.7M_\odot$ binary with the BA EoS. This is a high-mass system that produces a short-lived (∼2 ms) remnant, which collapses to a BH without a bounce (so it is classified as a system that promptly collapses even though BH formation is not "immediate"). The BA EoS is derived from a relativistic mean-field theory with parameters tweaked to produce an extremely large NS maximum mass while remaining consistent with current astronomical and laboratory constraints [62]. The $1.7M_\odot - 1.7M_\odot$ binary is just above the threshold mass of $M_{\rm thr} \simeq 3.38M_\odot$ for this EoS [40]. The proximity to the threshold mass and the extreme properties of the BA EoS are likely the reason why this binary is an outlier in Fig. 2 and in subsequent figures, where it is marked with a red square.

The existence of such a relation for BNS mergers is significant because it shows that the angular momentum of the remnant is primarily governed by the gravitational dynamics and is insensitive to the details of the hydrodynamics of these systems. Since the systems considered here are prompt collapses, the postmerger timescale is at most a few milliseconds, following which the remnant settles down into an isolated Kerr BH. As noted in Ref. [31], this relation can be used to calculate the final spin of the remnant BH, especially with next-generation detectors, which can measure the total radiated energy. Next-generation detectors may also be able to detect the quasinormal mode ringing of the remnant BH and measure the quasinormal mode frequency, providing an independent estimate of the final mass and spin. However, one needs to be cognizant that for unequal mass mergers, significant mass and angular momentum are contained in the accretion disk around the remnant BH [41,44,45,79] and need to be taken into account. A cross-validation of both measurements would be a crucial check of the dynamics near the merger when the gravitational radiation is maximum.

B. Remnant mass and spin

A Kerr black hole is formed from the prompt collapse of a quasicircular binary neutron star merger. For equal mass mergers, there is negligible accretion of matter around the collapsed BH. However, for unequal mass mergers, significant mass and angular momentum are contained in the accretion disk around the remnant BH [41,44,45,79]. The final mass M_f and dimensionless spin a_f of the remnant are estimated by (including the mass and angular momentum in the ejecta/disk)

$$M_f = M_{\rm adm} - E_{\rm rad}, \tag{3.2}$$

$$a_f = \frac{J_{\rm adm} - J_{\rm rad}}{M_f^2}, \tag{3.3}$$

where $M_{\rm adm}$ and $J_{\rm adm}$ are the Arnowitt–Deser–Misner (ADM) mass and angular momentum of the system at the beginning of the simulations. Note that the ADM mass differs from the total mass in that it also contains the energy of the gravitational field. For a binary system, the gravitational field energy includes the binding energy and the energy in gravitational waves. Figure 3 shows with unfilled markers the mass (left panel) and dimensionless spin (right panel) of the remnant (including the disk) for the set of binary configurations and EoSs considered in this study. It also shows in open circles the remnant properties for nonspinning BBHs having the same total mass and mass ratio as the BNS systems under consideration. The remnant mass and dimensionless spin in the case of BBH systems are calculated using the fitting formulas for initially nonspinning BBH given in Berti *et al.* [80]. The mass asymmetry of a system is depicted using a color gradient, with lighter shades of green representing more asymmetric binaries.

It is immediately clear that the remnant mass and dimensionless spin of promptly collapsing systems are larger than the corresponding BBH systems, signifying that less energy and angular momentum are radiated during the merger in the former compared to the latter. For a BBH merger, 3–4% of the total initial mass of the binary is radiated away in the form of gravitational waves, while for a BNS system that promptly collapses, only 1–2% of the initial total mass is radiated. Note that this is contrary to the case of a BNS merger forming a NS remnant, where the radiated energy is comparable to, though always less than, an equivalent BBH merger [81]. Moreover, for a BBH merger, the total mass of the system is a scaling factor, and the scaled final mass is a function of only the mass ratio, with a more asymmetric system radiating less energy. For a BNS merger, the total mass is not just a scaling factor, as is clear by the spread in M_f/M in Fig. 3. However, for a prompt collapse, this spread is very narrow and less than 1%. Due to this spread, there is no clear dependence on the mass ratio, even though the overall trend is that asymmetric systems radiate less for most cases.

The dimensionless final spin of an equal mass, initially nonspinning BBH system is ≈0.69, with the final spin decreasing for more asymmetric systems (see the right panel of Fig. 3). Again, the final spin depends only on the mass ratio of the system and not on the initial total mass.

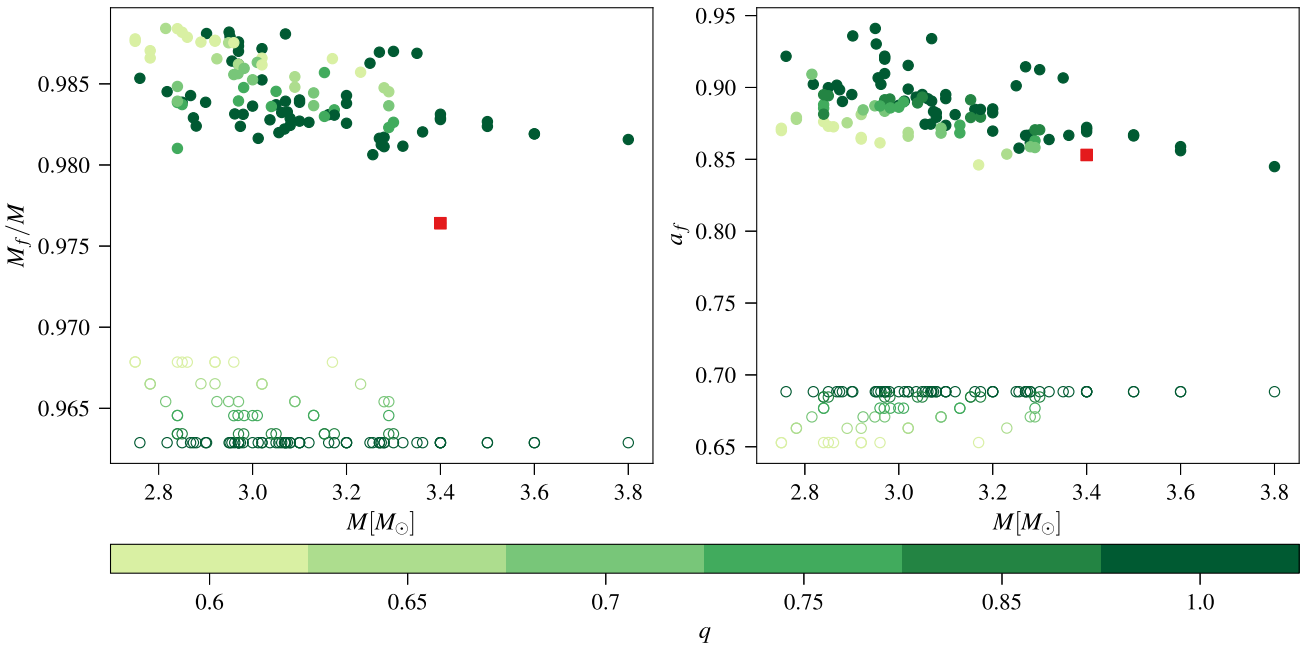

FIG. 3. Dimensionless final mass (left) and final spin (right) as a function of the total mass of the binary. Unfilled markers show the final mass and spin if the system were a binary black hole. The color gradient shows the asymmetry of the system, with lighter shades representing more asymmetric binaries. Note that the color bar is not uniform since simulations are only available at these fixed mass ratio values. The outlier denoted with a red square is the $1.7M_\odot - 1.7M_\odot$ with the BA EoS (see the main text for further discussion).

For the systems that promptly collapse, the smallest value of the dimensionless spin we find is $a_f \sim 0.85$, with the largest value reaching $a_f \sim 0.95$. Moreover, there is a spread in the values of the dimensionless final spin, which depends on the total mass of the system and the EoS. However, as in the case of the scaled final mass, the spread is narrow. Furthermore, one can qualitatively see that more asymmetric systems have lower final spin.

Motivated by the observation that the remnant mass and spin of prompt-collapse mergers (including the disk) differ from the equivalent BBH system, one can ask which BBH configurations produce analogous remnants. To probe this, we consider the catalog of publicly available noneccentric SXS simulations [82,83] of BBHs up to an inverse mass ratio of 3, since a BNS system is not expected to be more asymmetric. This gives us a set of 1937 BBH simulations containing nonspinning systems, aligned spin systems, and precessing systems. We plot them in the remnant mass–spin parameter space together with all the prompt-collapse mergers used in this study in Fig. 4. Astonishingly, we find that the two classes of sources lie in entirely disjointed areas of the parameter space. There is a tight negative correlation between the remnant mass and spin for BBH systems where the production of highly spinning remnants necessitates the loss of a large amount of energy through gravitational radiation. This is directly opposite to the trend seen in Fig. 2, where a smaller radiated energy means a larger remnant angular momentum. In fact, we find that the smallest scaled angular momentum ($J_f/M^2 = M_f^2 a_f/M^2$) of a prompt-collapse BNS remnant is greater than the largest value across all the BBH simulations considered (see the Appendix).

We calculated the mass ($m_{\rm disk}$) and the angular momentum ($J_{\rm disk}$) contained in the disk outside the apparent

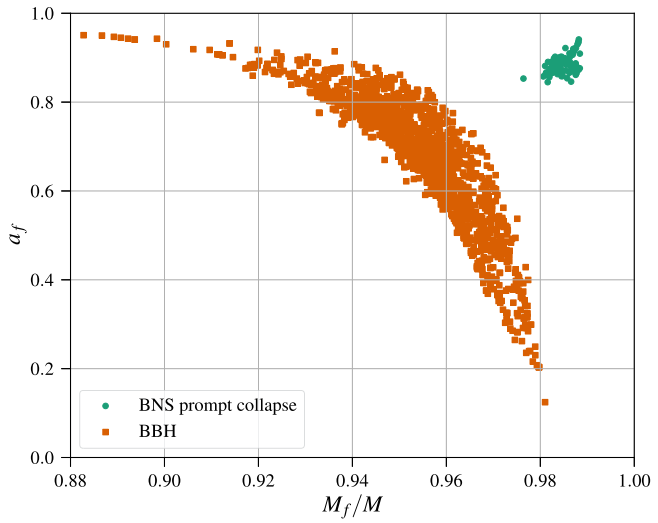

FIG. 4. The remnant mass and spin of BBH mergers versus BNS prompt collapses. There are 1937 BBH mergers in this figure corresponding to all the publicly available SXS simulations with $q \leq 3$ for which such information is available. The outlier denoted with a red square is the $1.7M_\odot - 1.7M_\odot$ with the BA EoS (see the main text for further discussion).

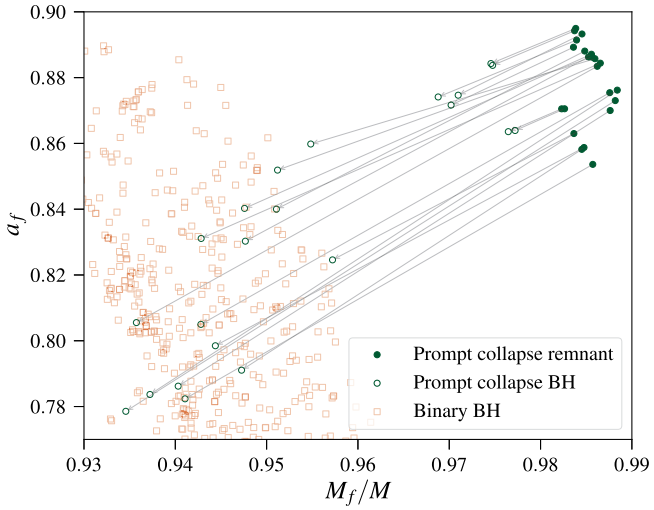

FIG. 5. The dimensionless mass and spin of the remnant, including the disk (filled circles), and only the remnant BH (open circles) for the subset of 22 simulations for which we extract the accretion disk properties. The arrows depict the link between the remnant (including the disk) and the BH. We also show the remnant mass and spin of BBH mergers (open squares) for reference.

horizon for a subset of 22 unequal mass simulations [79]. For these cases, the mass and dimensionless spin of the remnant BH can be estimated by

$$M_f^{\rm BH} = M_{\rm adm} - E_{\rm rad} - m_{\rm disk}, \tag{3.4}$$

$$a_f^{\rm BH} = \frac{J_{\rm adm} - J_{\rm rad} - J_{\rm disk}}{M_f^2}. \tag{3.5}$$

We contrast the remnant properties of such systems with those of the remnant BHs in Fig. 5. We observe that there is a significant spread in the properties of the final BHs, even though the remnants are tightly clustered. Indeed, the most asymmetric ones lie within the cluster of the BBH merger remnants. Nevertheless, it is worth remembering that the spacetime around the remnant BH is different from the BBH case due to the presence of an accretion disk. Note that some of the accreting matter will fall back into the BH on timescales of $\mathcal{O}(s)$ while the disk properties are extracted on timescales of $\mathcal{O}(ms)$. Therefore, at large timescales, the BH properties will be somewhere in between those of the remnants and corresponding BHs depicted in Fig. 5.

C. Implications of GW230529 on NS EoS

GW230529 [84] is the merger of a compact object with mass $3.6M_\odot$ and an NS of mass $1.4M_\odot$. The nature of the primary component is uncertain. It could be either the heaviest NS or the lightest BH observed to date. The formation channel for such an object is unclear as well. One of the possibilities is that it formed from a previous generation BNS merger [85]. Interestingly, it is spinning with a spin magnitude of $0.44^{+0.40}_{-0.37}$, and this allows us to make statements about the EoS of NS based on the discussion above.

Recall that $M_{\rm thr}$, the minimum total mass of a binary undergoing prompt collapse, is proportional to the maximum mass of a cold, nonrotating NS, i.e., $M_{\rm thr} = k_{\rm thr} M_{\rm max}$, $k_{\rm thr} \in [1.2, 1.6]$ [40]. From Fig. 5, we can calculate the maximum total mass of the first-generation BNS mergers—accounting for the energy released by the binary inspiral and merger—to be $< 3.6/0.935 \approx 3.85M_\odot$. Note that we also assume that the accretion disk does not fall back into the BH following the first-generation merger. This gives the maximum threshold mass, $M_{\rm thr} \lesssim 3.85M_\odot$. If this first-generation merger underwent prompt collapse, that would imply $M_{\rm max} \lesssim 3.85/1.2 \approx 3.21M_\odot$. On the other hand, if the binary progenitor of the primary in GW230529 did not undergo prompt collapse, that would constrain the minimum maximum mass to be $M_{\rm max} \gtrsim 3.85/1.6 \approx 2.41M_\odot$. This latter scenario would be favored for small spins of the primary component of GW230529, in light of the results discussed in this work. This highlights the potential to use precise spin measurements to constrain the NS EoS.

D. Detectability of the postmerger

It is instructive to calculate the expected signal-to-noise ratio (SNR) in the postmerger for the systems in our simulations. To this effect, we consider a 40 km Cosmic Explorer detector as a reference and place binaries at a distance of 100 Mpc. We expect to observe 2–3 BNS mergers from within a volume of radius 100 Mpc per year [14] based on the median rate of BNS mergers from the second Gravitational Wave Transient Catalog [86]. We assume that a binary is optimally located and oriented with respect to the detector. The postmerger SNRs for such systems are then calculated using the formula

$$\rho^2 = 4 \int_{f_{\rm lo}}^{f_{\rm hi}} \frac{|\tilde{h}(f)|^2}{S_h(f)} df, \tag{3.6}$$

where $\tilde{h}(f) = F_+ h_+ + F_\times h_\times$, F_+ and $F_\times$ are the antenna pattern functions of the detector, and h_+ and $h_\times$ are the two gravitational wave polarizations that we obtain from numerical relativity simulations. In practice, for an optimal location in the sky with respect to the detector, we choose $F_+ = 1$, and $F_\times = 0$. $S_h(f)$ is the noise power spectral density of the detector.

The postmerger SNR is very sensitive to the choice of the lower-frequency cutoff since it lies at the heart of the sensitive band of the detector. We find that the merger frequency calculated directly from the NR data[1] varied significantly from those predicted by the NR fits in Gonzalez *et al.* [66] and Dietrich *et al.* [87]. The fits

[1]The merger frequency is defined as the instantaneous frequency corresponding to the peak amplitude of the $\ell = 2$, $m = 2$ mode of the strain.

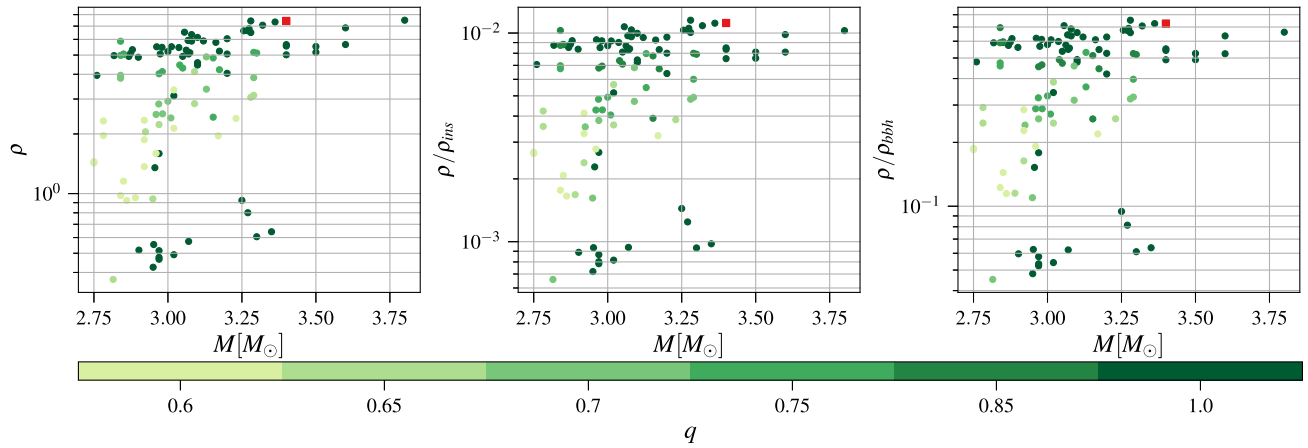

FIG. 6. Left: the SNR in the postmerger signal for the systems considered in this study, placed at a distance of 100 Mpc and optimally oriented for a 40 km Cosmic Explorer detector. Center: the SNR in the postmerger as a fraction of the inspiral SNR. Right: the SNR in the postmerger as a fraction of an equivalent BBH postmerger. As discussed in the main text, we separate the inspiral and postmerger signals using the cutoff frequency of 2048 Hz. The color gradient shows the asymmetry of the system, with lighter shades representing more asymmetric binaries. Note that the color bar is not uniform since simulations are only available at these fixed mass ratio values. The binary denoted with a red square is the $1.7M_\odot - 1.7M_\odot$ with the BA EoS (see the main text for further discussion).

themselves varied considerably across a wide swath of the parameter space. Therefore, we make the choice to define the postmerger from a fixed $f_{\rm lo} = 2048$ Hz. The high-frequency cutoff is taken to be $f_{\rm hi} = 7000$ Hz.

In the left panel of Fig. 6, we show the postmerger SNRs for the binaries we consider. We find that most of them have SNRs greater than 4. These are also equal mass or nearly equal mass binaries. Given that these are very short signals with extremely loud inspirals, even an SNR of 4 detection of such a signal will have a very small *false alarm rate* and allow for reliable parameter estimation. For instance, GW150914 had a ringdown SNR of ∼4.8 (∼8.5) starting 6.5 ms (3 ms) after merger and a base-10-log Bayes factor $\log_{10}\mathcal{B}$ of ∼3.5 (∼14) for a damped sinusoid model of the ringdown against Gaussian noise [88]. The comparatively asymmetric binaries, as distinguished by their lighter shades in the figure, have SNRs between 0.9 and 4. However, we also find a select few (almost) equal mass binaries with a tiny postmerger SNR. These binaries "shut off" immediately after their merger, and there is no discernible postmerger radiation from them, hence why they have such small SNRs.

In addition to the postmerger SNR, we calculate the SNR in the inspiral for all binaries, where we take the starting lower frequency to be $f_{\rm lo,insp} = 5$ Hz and the high-frequency cutoff to be $f_{\rm hi,insp} = 2048$ Hz. We do not consider tidal effects in the amplitude of the inspiral waveform and, as a result, the SNR in the inspiral for an optimally located face-on system is given by

$$\rho^2 = \frac{5}{6\pi^{4/3}} \frac{\mathcal{M}_c^{5/3}}{D_L^2} \int_{f_{\rm lo,insp}}^{f_{\rm hi,insp}} \frac{f^{-7/3}}{S_h(f)} df, \tag{3.7}$$

where $\mathcal{M}_c = (m_1 m_2)^{3/5}/(m_1 + m_2)^{1/5}$ is the chirp mass of the binary.

We show the ratio of the SNR in the postmerger to the inspiral in the central panel of Fig. 6. We find that for a majority of the systems considered, the postmerger has ∼0.5–1% of the inspiral SNR, and for a select few, it is much lower at $\lesssim$0.1%.

Finally, we compare the postmerger SNR of the prompt-collapse BNS merger to the equivalent BBH mergers. The SNR is calculated in the same frequency range of [2048, 7000] Hz as for the BNS postmerger for an equivalent comparison. The BBH waveform model is chosen to be IMRPhenomD [22,89], which is a nonprecessing waveform model containing only the $(l, |m|) = (2, 2)$ mode.

We show the ratio of the SNRs in the prompt-collapse ringdown to the BBH ringdown in the right panel of Fig. 6. We find that the SNR for BNS is always smaller than the corresponding BBH system. For a majority of the systems, the BNS postmerger SNR is 40%–80% of the BBH equivalent. However, for relatively asymmetric binaries, this can be even lower and, in some cases, contains only 10% of the SNR of their BBH counterparts. Unsurprisingly, for systems with a negligible postmerger signal, the fractional SNR is only a few percent. The smaller SNR for systems that promptly collapse is expected from the previous section, where it is shown that these systems are poorer GW emitters than BBHs. The lack of power in the ringdown signal can be smoking gun evidence for a BNS system leading to a prompt collapse [46]. We note that the long-wavelength approximation for the detector response assumed in our calculations needs to be relaxed in future studies. The approximation is valid for up to about a frequency of 1000 Hz and, therefore, for the inspiral.

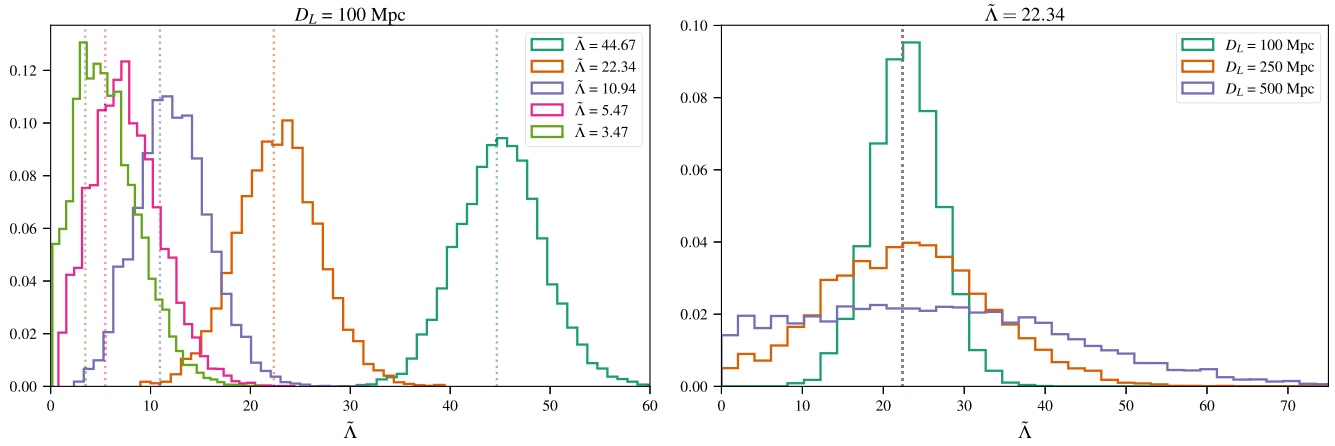

FIG. 7. The probability density functions on the reduced tidal deformability parameter, $\tilde{\Lambda}$, with a 40 km Cosmic Explorer detector for a binary with redshifted masses $(2.0M_\odot, 1.9M_\odot)$. Left: the sources are kept at a fixed distance $D_L = 100$ Mpc but the tidal deformabilities are varied. Right: the reduced tidal deformability is kept constant at $\tilde{\Lambda} = 22.34$ but the distance to the source is varied.

However, at higher frequencies, the antenna pattern functions become frequency dependent, and hence an optimal orientation is signal dependent. Furthermore, Ref. [79] finds that the SNR computed using the long-wavelength approximation could be overestimated by a factor of ≈4 for the types of signals considered here.

Across the three panels, we find that the locations of the binaries are approximately constant, while the scale on the y-axis varies. This is because there is minimal variability in the BNS inspiral SNR or the BBH postmerger SNR across the different binary configurations.

E. Distinguishing BNS versus BBH from postmerger

In this section, we consider the distinguishability of a BNS and BBH merger using their postmerger signal if their inspiral is consistent with each other. To answer this, we first try to find the minimum tidal deformability parameter $\tilde{\Lambda}$ for which $\tilde{\Lambda} = 0$ is excluded at a high confidence. We carry out an injection analysis with a set of high-mass, nonspinning, BNS signals modeled using the IMRPhenomPv2_NRTidalv2 [22,90,91] waveform model assuming a single 40 km Cosmic Explorer detector. We choose the sky location and orientation of the binaries as that of GW170817 and the redshifted masses to be $(2.0M_\odot, 1.9M_\odot)$. We vary only the tidal deformabilities and the distance to the sources across the set. Our set of injected binaries can be divided into two nonmutually exclusive subsets. Set 1 contains four injections at $D_L = 100$ Mpc with varying $\tilde{\Lambda} = \{44.67, 22.34, 10.94, 5.47, 3.47\}$. Set 2 contains three simulations with fixed $\tilde{\Lambda} = 22.34$ at varying luminosity distances of $D_L = \{100, 250, 500\}$ Mpc. We note that these values for the tidal deformability do not correspond to any named EoS but were rather chosen by hand. We stress that this is inconsequential as long as the choices are in the ballpark of the EoS uncertainty. We use the publicly available GW simulation package BILBY [92,93] to inject and recover the signal in zero noise. We assume the binary's position in the sky is known since we are primarily interested in the tidal parameters, which are minimally correlated with the extrinsic parameters, such as the sky position. We sample over all the other parameters of a nonspinning binary using the PyMultiNest [94] sampler and impose standard priors on all parameters, notably a uniform prior on the tidal deformability parameter $\tilde{\Lambda}$.

The 1D marginalized posteriors on $\tilde{\Lambda}$ from parameter estimation across the two subsets of injections are shown in Fig. 7. The simulations corresponding to the binaries in Set 1 are shown in the left panel, while those corresponding to the binaries in Set 2 are depicted in the right panel. We find that a compact binary merger at $D_L = 100$ Mpc can be confidently classified as a BNS merger using its $\tilde{\Lambda}$ measurement for a value as small as $\tilde{\Lambda} \sim 5$ and even $\tilde{\Lambda} \approx 3.5$ can exclude 0 at $> 70\%$ confidence. Only a single EoS (SRO1) among the set of EoSs we have considered attains a Λ value smaller than 4 for an NS mass of $\sim 2.3M_\odot$. An equal mass binary with a component mass of $2.3M_\odot$ would have a larger SNR than other masses considered in this analysis, so it would probably exclude 0 at an even higher confidence level. Therefore, up to a distance of $D_L = 100$ Mpc, the inspiral signal can distinguish virtually all BNS mergers from BBH mergers.

Next, we look at how the $\tilde{\Lambda}$ errors vary with distance. From the right panel of Fig. 7, we find that a $\tilde{\Lambda} \approx 22$ can be measured to exclude the value 0 at a distance of $D_L = 250$ Mpc. For larger distances, the $\tilde{\Lambda}$ posterior will exclude 0 at smaller confidence levels, as can be seen from the histogram of the same source placed at $D_L = 500$ Mpc, and it will be difficult to conclusively identify such events

as NS mergers. Moreover, at distances of 250 Mpc and 500 Mpc, the SNRs in the prompt-collapse ringdowns will be smaller by factors of 2.5 and 5, as compared to the values shown in Fig. 6. Neither BNS nor BBH ringdown will be clearly observable at such distances, and hence a simple comparison of signal power in the ringdown cannot differentiate these systems. In such a scenario, accurate waveform templates describing the full signal are required to extract maximum information from the data and possibly distinguish them.

IV. CONCLUSION AND DISCUSSION

The gravitational wave spectrum following a BNS merger that does not collapse has a rich phenomenology that is very sensitive to the EoS used. Although there is a broad consensus on certain features of the postmerger spectrum, such a signal is not well modeled for faithful parameter estimation and reconstruction. On the other hand, prompt-collapse BNS mergers contain complementary and largely EoS-agnostic information and can determine NS features, such as the maximum mass supported by the NS EoS and the properties of the accretion disk around the remnant BH. To that end, we analyze 107 prompt-collapse mergers across a set of EoSs, total mass, and mass ratios.

We calculate the total energy radiated in gravitational waves and observe that it is very closely related to the angular momentum of the remnant. We verify that this relationship closely follows the relation proposed in Zappa *et al.* [31] and discuss its implications.

We find that BNS prompt collapses are poor GW emitters compared to their BBH equivalent. We report that the spread in the scaled final mass and the dimensionless final spin across all the simulations considered is very narrow. This is possibly due to the minimal role played by the EoS in determining the dynamics of the very short prompt-collapse timescale. We also observe that the final mass and spin of the remnant are larger than the product of an equivalent BBH merger with the same initial configuration. In fact, the remnants are highly spinning with dimensionless spins between $0.85 < a_f < 0.95$. While for unequal mass systems, a portion of the mass and angular momentum is contained in the accretion disk surrounding the remnant BH, equal mass mergers have minimal matter accretion. Such systems can be of great astrophysical interest since it is otherwise difficult to produce highly spinning black holes. One can produce highly spinning BH remnants in a BBH merger, but then one also has to start with relatively high spins for the progenitors, with the two values approaching each other the larger they become [95,96]. An interesting avenue to explore is whether extremely high remnant spins can be achieved using BNS mergers. This offers the exciting possibility of studying superradiance resonance cavities outside rapidly rotating BHs [97]. Preliminary investigations suggest that the additional angular momentum from progenitor spins is predominantly transferred to the accretion disk [98–103]. We intend to explore this in the future.

We calculate the postmerger SNR of prompt-collapse BNS mergers in the frequency band [2048, 7000] Hz and compare them to the signal strength of an equivalent BBH postmerger. We report that the majority of the systems considered have postmerger SNRs 40%–80% relative to a BBH postmerger, with some as low as a few percent. We find that a majority of these systems would be observable up to a distance of 100 Mpc with a future 40 km CE.

We examine the distinguishability of massive BNS mergers with small tidal deformabilities that could result in prompt collapse from BBH systems. We find that reduced tidal deformabilities as small as $\tilde{\Lambda} \approx 3.5$ can be measured to exclude 0 up to a distance of 100 Mpc and $\tilde{\Lambda} \approx 22$ to distances $\sim$250 Mpc.

Finally, we discuss the NS EoS implications of associating a prompt collapse with the progenitor of GW230529's primary component. We find that the maximum mass of NS is bound from above to $\lesssim 3.21 M_\odot$ if the primary is highly spinning, while it is constrained from below to $\gtrsim 2.41 M_\odot$ if it is not. These have implications on the maximum mass of a NS [40].

Our work lays out the extremely interesting NS and GW physics in the 4 kHz–10 kHz region, which is often not the focus of technology and is only narrowly accessible to currently proposed GW detectors.

A limitation of our study is that we use the long-wavelength approximation for the detector response for both SNR calculations and parameter estimation. We plan to relax this assumption in the future. Another limitation of the study presented here is that only NR simulations with irrotational initial data are considered, although astrophysical BNSs are expected to be slowly spinning. We plan to extend the study to spinning BNSs and determine the maximal remnant BH spin that can be produced in a BNS merger. It would also be interesting to understand the distribution of remnant properties for various configurations of black hole–neutron star binaries. We leave that to the future as well.

ACKNOWLEDGMENTS

We thank Aditya Vijaykumar for useful discussions. A. D. is supported by the National Science Foundation (NSF) Grant No. PHY-2012083. D. R. acknowledges funding from NSF under Grants No. PHY-2020275, No. PHY-2116686, No. AST-2108467, and No. PHY-2407681, the Sloan Foundation, and from the U.S. Department of Energy, Office of Science, Division of Nuclear Physics under Awards No. DE-SC0021177 and

No. DE-SC0024388. B. S. S. acknowledges NSF Grants No. AST-2307147, No. PHY-2207638, No. PHY-2308886, and No. PHY-2309064.

DATA AVAILABILITY

The data that support the findings of this article are not publicly available upon publication because it is not technically feasible and/or the cost of preparing, depositing, and hosting the data would be prohibitive within the terms of this research project. The data are available from the authors upon reasonable request.

APPENDIX: REMNANT MASS-SPIN

Figure 8 shows the angular momentum of the remnant scaled by the total mass of the binary for prompt collapses and BBH mergers up to a mass ratio of 3 (see Sec. III B for more details). It is observed that the angular momentum of the prompt-collapse remnant per unit total mass is always greater than what is possible to achieve with BBH. Note that the BBH systems contain aligned spin and precessing binaries too.

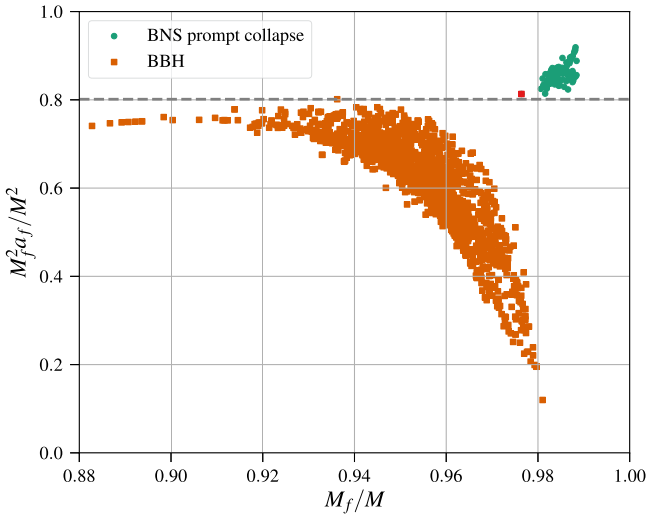

FIG. 8. The remnant mass and angular momentum (J_f/M^2) of BBH mergers versus BNS prompt collapses. There are 1937 BBH mergers in this figure corresponding to all the publicly available SXS simulations with $q \leq 3$ for which such information is available. The outlier denoted with a red square is the $1.7M_\odot - 1.7M_\odot$ with the BA EoS (see the main text for further discussion).

[1] B. P. Abbott *et al.* (LIGO Scientific Collaboration and Virgo Collaboration), Observation of gravitational waves from a binary black hole merger, Phys. Rev. Lett. **116**, 061102 (2016).
[2] R. Abbott *et al.* (KAGRA Collaboration, VIRGO Collaboration, and LIGO Scientific Collaboration), GWTC-3: Compact binary coalescences observed by LIGO and Virgo during the second part of the third observing run, Phys. Rev. X **13**, 041039 (2023).
[3] R. Abbott *et al.* (LIGO Scientific Collaboration, VIRGO Collaboration, and KAGRA Collaboration), Tests of general relativity with GWTC-3, arXiv:2112.06861.
[4] B. P. Abbott *et al.* (LIGO Scientific Collaboration and Virgo Collaboration), Tests of general relativity with GW170817, Phys. Rev. Lett. **123**, 011102 (2019).
[5] B. P. Abbott *et al.* (LIGO Scientific, Virgo, 1M2H, Dark Energy Camera GW-E, DES, DLT40, Las Cumbres Observatory, VINROUGE, and MASTER Collaborations), A gravitational-wave standard siren measurement of the Hubble constant, Nature (London) **551**, 85 (2017).
[6] R. Abbott *et al.* (LIGO Scientific Collaboration, Virgo Collaboration, and KAGRA Collaboration), Constraints on the cosmic expansion history from GWTC–3, Astrophys. J. **949**, 76 (2023).
[7] B. P. Abbott *et al.* (LIGO Scientific Collaboration and Virgo Collaboration), Model comparison from LIGO–Virgo data on GW170817's binary components and consequences for the merger remnant, Classical Quantum Gravity **37**, 045006 (2020).
[8] J. Aasi *et al.* (LIGO Scientific Collaboration), Advanced LIGO, Classical Quantum Gravity **32**, 074001 (2015).
[9] F. Acernese *et al.* (VIRGO Collaboration), Advanced Virgo: A second-generation interferometric gravitational wave detector, Classical Quantum Gravity **32**, 024001 (2015).
[10] T. Akutsu *et al.* (KAGRA Collaboration), KAGRA: 2.5 generation interferometric gravitational wave detector, Nat. Astron. **3**, 35 (2019).
[11] D. Reitze *et al.*, Cosmic explorer: The U.S. contribution to gravitational-wave astronomy beyond LIGO, Bull. Am. Astron. Soc. **51**, 035 (2019).
[12] M. Punturo *et al.*, The third generation of gravitational wave observatories and their science reach, Classical Quantum Gravity **27**, 084007 (2010).
[13] R. X. Adhikari *et al.* (LIGO Collaboration), A cryogenic silicon interferometer for gravitational-wave detection, Classical Quantum Gravity **37**, 165003 (2020).
[14] S. Borhanian and B. S. Sathyaprakash, Listening to the Universe with next generation ground-based gravitational-wave detectors, Phys. Rev. D **110**, 083040 (2024).
[15] F. Iacovelli, M. Mancarella, S. Foffa, and M. Maggiore, Forecasting the detection capabilities of third-generation gravitational-wave detectors using GWFAST, Astrophys. J. **941**, 208 (2022).
[16] A. Abac *et al.*, The science of the Einstein telescope, arXiv:2503.12263.
[17] M. Punturo *et al.*, The Einstein telescope: A third-generation gravitational wave observatory, Classical Quantum Gravity **27**, 194002 (2010).

[18] M. Evans *et al.*, A horizon study for cosmic explorer: Science, observatories, and community, arXiv:2109.09882.

[19] I. Gupta *et al.*, Characterizing gravitational wave detector networks: from $A^\sharp$ to cosmic explorer, Classical Quantum Gravity **41**, 245001 (2024).

[20] M. Branchesi *et al.*, Science with the Einstein telescope: A comparison of different designs, J. Cosmol. Astropart. Phys. 07 (2023) 068.

[21] M. Evans *et al.*, Cosmic explorer: A submission to the NSF MPSAC ngGW subcommittee, arXiv:2306.13745.

[22] S. Khan, S. Husa, M. Hannam, F. Ohme, M. Pürrer, X. Jiménez Forteza, and A. Bohé, Frequency-domain gravitational waves from nonprecessing black-hole binaries. II. A phenomenological model for the advanced detector era, Phys. Rev. D **93**, 044007 (2016).

[23] R. Huxford, R. Kashyap, S. Borhanian, A. Dhani, I. Gupta, and B. S. Sathyaprakash, Accuracy of neutron star radius measurement with the next generation of terrestrial gravitational-wave observatories, Phys. Rev. D **109**, 103035 (2024).

[24] B. P. Abbott *et al.* (LIGO Scientific Collaboration and Virgo Collaboration), GW170817: Observation of gravitational waves from a binary neutron star inspiral, Phys. Rev. Lett. **119**, 161101 (2017).

[25] B. P. Abbott *et al.* (LIGO Scientific Collaboration and Virgo Collaboration), GW190425: Observation of a compact binary coalescence with total mass $\sim 3.4 M_\odot$, Astrophys. J. Lett. **892**, L3 (2020).

[26] B. P. Abbott *et al.* (LIGO Scientific, Virgo, Fermi GBM, INTEGRAL, IceCube, AstroSat Cadmium Zinc Telluride Imager Team, IPN, Insight-Hxmt, ANTARES, Swift, AGILE Team, 1M2H Team, Dark Energy Camera GW-EM, DES, DLT40, GRAWITA, Fermi-LAT, ATCA, ASKAP, Las Cumbres Observatory Group, OzGrav, DWF (Deeper Wider Faster Program), AST3, CAASTRO, VINROUGE, MASTER, J-GEM, GROWTH, JAGWAR, CaltechNRAO, TTU-NRAO, NuSTAR, Pan-STARRS, MAXI Team, TZAC Consortium, KU, Nordic Optical Telescope, ePESSTO, GROND, Texas Tech University, SALT Group, TOROS, BOOTES, MWA, CALET, IKI-GW Follow-up, H.E.S.S., LOFAR, LWA, HAWC, Pierre Auger, ALMA, Euro VLBI Team, Pi of Sky, Chandra Team at McGill University, DFN, ATLAS Telescopes, High Time Resolution Universe Survey, RIMAS, RATIR, and SKA South Africa/MeerKAT Collaborations), Multi-messenger observations of a binary neutron star merger, Astrophys. J. Lett. **848**, L12 (2017).

[27] J. M. Lattimer, The nuclear equation of state and neutron star masses, Annu. Rev. Nucl. Part. Sci. **62**, 485 (2012).

[28] S. A. Hughes and K. Menou, Golden binaries for LISA: Robust probes of strong-field gravity, Astrophys. J. **623**, 689 (2005).

[29] A. Ghosh *et al.*, Testing general relativity using golden black-hole binaries, Phys. Rev. D **94**, 021101 (2016).

[30] A. Gupta *et al.*, Possible causes of false general relativity violations in gravitational wave observations, SciPost Phys. Community Rep. **5** (2024).

[31] F. Zappa, S. Bernuzzi, D. Radice, A. Perego, and T. Dietrich, Gravitational-wave luminosity of binary neutron stars mergers, Phys. Rev. Lett. **120**, 111101 (2018).

[32] M. Shibata, K. Taniguchi, and K. Uryu, Merger of binary neutron stars with realistic equations of state in full general relativity, Phys. Rev. D **71**, 084021 (2005).

[33] A. Perego, D. Logoteta, D. Radice, S. Bernuzzi, R. Kashyap, A. Das, S. Padamata, and A. Prakash, Probing the incompressibility of nuclear matter at ultrahigh density through the prompt collapse of asymmetric neutron star binaries, Phys. Rev. Lett. **129**, 032701 (2022).

[34] K. Hotokezaka, K. Kyutoku, H. Okawa, M. Shibata, and K. Kiuchi, Binary neutron star mergers: Dependence on the nuclear equation of state, Phys. Rev. D **83**, 124008 (2011).

[35] A. Bauswein, T. W. Baumgarte, and H. T. Janka, Prompt merger collapse and the maximum mass of neutron stars, Phys. Rev. Lett. **111**, 131101 (2013).

[36] M. Agathos, F. Zappa, S. Bernuzzi, A. Perego, M. Breschi, and D. Radice, Inferring prompt black-hole formation in neutron star mergers from gravitational-wave data, Phys. Rev. D **101**, 044006 (2020).

[37] S. Köppel, L. Bovard, and L. Rezzolla, A general-relativistic determination of the threshold mass to prompt collapse in binary neutron star mergers, Astrophys. J. Lett. **872**, L16 (2019).

[38] A. Bauswein, S. Blacker, V. Vijayan, N. Stergioulas, K. Chatziioannou, J. A. Clark, N.-U. F. Bastian, D. B. Blaschke, M. Cierniak, and T. Fischer, Equation of state constraints from the threshold binary mass for prompt collapse of neutron star mergers, Phys. Rev. Lett. **125**, 141103 (2020).

[39] A. Bauswein, S. Blacker, G. Lioutas, T. Soultanis, V. Vijayan, and N. Stergioulas, Systematics of prompt black-hole formation in neutron star mergers, Phys. Rev. D **103**, 123004 (2021).

[40] R. Kashyap *et al.*, Numerical relativity simulations of prompt collapse mergers: Threshold mass and phenomenological constraints on neutron star properties after GW170817, Phys. Rev. D **105**, 103022 (2022).

[41] M. Kölsch, T. Dietrich, M. Ujevic, and B. Bruegmann, Investigating the mass-ratio dependence of the prompt-collapse threshold with numerical-relativity simulations, Phys. Rev. D **106**, 044026 (2022).

[42] K. A. Çokluk, K. Yakut, and B. Giacomazzo, General relativistic simulations of high-mass binary neutron star mergers: Rapid formation of low-mass stellar black holes, Mon. Not. R. Astron. Soc. **527**, 8043 (2023).

[43] F. Özel and P. Freire, Masses, radii, and the equation of state of neutron stars, Annu. Rev. Astron. Astrophys. **54**, 401 (2016).

[44] A. Camilletti, L. Chiesa, G. Ricigliano, A. Perego, L. C. Lippold, S. Padamata, S. Bernuzzi, D. Radice, D. Logoteta, and F. M. Guercilena, Numerical relativity simulations of the neutron star merger GW190425: Microphysics and mass ratio effects, Mon. Not. R. Astron. Soc. **516**, 4760 (2022).

[45] R. Dudi, A. Adhikari, B. Brügmann, T. Dietrich, K. Hayashi, K. Kawaguchi, K. Kiuchi, K. Kyutoku, M. Shibata, and W. Tichy, Investigating GW190425 with

numerical-relativity simulations, Phys. Rev. D **106**, 084039 (2022).
[46] A. Dhani, D. Radice, J. Schütte-Engel, S. Gardner, B. Sathyaprakash, D. Logoteta, A. Perego, and R. Kashyap, Prospects for direct detection of black hole formation in neutron star mergers with next-generation gravitational-wave detectors, Phys. Rev. D **109**, 044071 (2024).
[47] S. Banik, M. Hempel, and D. Bandyopadhyay, New hyperon equations of state for supernovae and neutron stars in density-dependent hadron field theory, Astrophys. J. Suppl. Ser. **214**, 22 (2014).
[48] I. Bombaci and D. Logoteta, Equation of state of dense nuclear matter and neutron star structure from nuclear chiral interactions, Astron. Astrophys. **609**, A128 (2018).
[49] D. Logoteta, A. Perego, and I. Bombaci, Microscopic equation of state of hot nuclear matter for numerical relativity simulations, Astron. Astrophys. **646**, A55 (2021).
[50] D. Logoteta, I. Bombaci, and A. Perego, Isoentropic equations of state of β-stable hadronic matter with a quark phase transition, Eur. Phys. J. A **58**, 55 (2022).
[51] S. Typel, G. Ropke, T. Klahn, D. Blaschke, and H. H. Wolter, Composition and thermodynamics of nuclear matter with light clusters, Phys. Rev. C **81**, 015803 (2010).
[52] M. Hempel and J. Schaffner-Bielich, Statistical model for a complete supernova equation of state, Nucl. Phys. **A837**, 210 (2010).
[53] J. M. Lattimer and F. D. Swesty, A generalized equation of state for hot, dense matter, Nucl. Phys. **A535**, 331 (1991).
[54] A. W. Steiner, M. Hempel, and T. Fischer, Core-collapse supernova equations of state based on neutron star observations, Astrophys. J. **774**, 17 (2013).
[55] F. Douchin and P. Haensel, A unified equation of state of dense matter and neutron star structure, Astron. Astrophys. **380**, 151 (2001).
[56] A. S. Schneider, L. F. Roberts, and C. D. Ott, Open-source nuclear equation of state framework based on the liquid-drop model with Skyrme interaction, Phys. Rev. C **96**, 065802 (2017).
[57] A. S. Schneider, L. F. Roberts, C. D. Ott, and E. O'connor, Equation of state effects in the core collapse of a 20-$M_\odot$ star, Phys. Rev. C **100**, 055802 (2019).
[58] M. Alford, M. Braby, M. W. Paris, and S. Reddy, Hybrid stars that masquerade as neutron stars, Astrophys. J. **629**, 969 (2005).
[59] N. K. Glendenning and S. A. Moszkowski, Reconciliation of neutron star masses and binding of the lambda in hypernuclei, Phys. Rev. Lett. **67**, 2414 (1991).
[60] B. D. Lackey, M. Nayyar, and B. J. Owen, Observational constraints on hyperons in neutron stars, Phys. Rev. D **73**, 024021 (2006).
[61] J. S. Read, B. D. Lackey, B. J. Owen, and J. L. Friedman, Constraints on a phenomenologically parameterized neutron-star equation of state, Phys. Rev. D **79**, 124032 (2009).
[62] F. J. Fattoyev, C. J. Horowitz, J. Piekarewicz, and B. Reed, GW190814: Impact of a 2.6 solar mass neutron star on the nucleonic equations of state, Phys. Rev. C **102**, 065805 (2020).
[63] A. Bauswein, H.-T. Janka, and R. Oechslin, Testing approximations of thermal effects in neutron star merger simulations, Phys. Rev. D **82**, 084043 (2010).
[64] A. Endrizzi, D. Logoteta, B. Giacomazzo, I. Bombaci, W. Kastaun, and R. Ciolfi, Effects of chiral effective field theory equation of state on binary neutron star mergers, Phys. Rev. D **98**, 043015 (2018).
[65] A. Figura, J.-J. Lu, G. F. Burgio, Z.-H. Li, and H.-J. Schulze, Hybrid equation of state approach in binary neutron-star merger simulations, Phys. Rev. D **102**, 043006 (2020).
[66] A. Gonzalez *et al.*, Second release of the CoRe database of binary neutron star merger waveforms, Classical Quantum Gravity **40**, 085011 (2023).
[67] E. Gourgoulhon, P. Grandclement, K. Taniguchi, J.-A. Marck, and S. Bonazzola, Quasiequilibrium sequences of synchronized and irrotational binary neutron stars in general relativity: 1. Method and tests, Phys. Rev. D **63**, 064029 (2001).
[68] D. Radice and L. Rezzolla, THC: A new high-order finite-difference high-resolution shock-capturing code for special-relativistic hydrodynamics, Astron. Astrophys. **547**, A26 (2012).
[69] D. Radice, L. Rezzolla, and F. Galeazzi, Beyond second-order convergence in simulations of binary neutron stars in full general-relativity, Mon. Not. R. Astron. Soc. **437**, L46 (2014).
[70] D. Radice, L. Rezzolla, and F. Galeazzi, High-order fully general-relativistic hydrodynamics: New approaches and tests, Classical Quantum Gravity **31**, 075012 (2014).
[71] D. Radice, L. Rezzolla, and F. Galeazzi, High-order numerical-relativity simulations of binary neutron stars, ASP Conf. Ser. **498**, 121 (2015).
[72] R. Haas *et al.*, The Einstein Toolkit (2022), to find out more, visit http://einsteintoolkit.org.
[73] E. Schnetter, S. H. Hawley, and I. Hawke, Evolutions in 3-D numerical relativity using fixed mesh refinement, Classical Quantum Gravity **21**, 1465 (2004).
[74] C. Reisswig, R. Haas, C. D. Ott, E. Abdikamalov, P. Mösta, D. Pollney, and E. Schnetter, Three-dimensional general-relativistic hydrodynamic simulations of binary neutron star coalescence and stellar collapse with multipatch grids, Phys. Rev. D **87**, 064023 (2013).
[75] M. J. Berger and J. Oliger, Adaptive mesh refinement for hyperbolic partial differential equations, J. Comput. Phys. **53**, 484 (1984).
[76] M. J. Berger and P. Colella, Local adaptive mesh refinement for shock hydrodynamics, J. Comput. Phys. **82**, 64 (1989).
[77] T. Damour, A. Nagar, D. Pollney, and C. Reisswig, Energy versus angular momentum in black hole binaries, Phys. Rev. Lett. **108**, 131101 (2012).
[78] F. Zappa (Private communication).
[79] A. Dhani, A. Camilletti, A. L. De Santis, A. Cozzumbo, D. Radice, D. Logoteta, A. Perego, J. Harms, and M. Branchesi, Direct measurement of the accretion disk formed in prompt collapse mergers with future gravitational-wave observatories, arXiv:2507.14071.
[80] E. Berti, V. Cardoso, J. A. Gonzalez, U. Sperhake, M. Hannam, S. Husa, and B. Bruegmann, Inspiral, merger and

ringdown of unequal mass black hole binaries: A multipolar analysis, Phys. Rev. D **76**, 064034 (2007).
[81] S. Bernuzzi, D. Radice, C. D. Ott, L. F. Roberts, P. Moesta, and F. Galeazzi, How loud are neutron star mergers?, Phys. Rev. D **94**, 024023 (2016).
[82] M. Boyle *et al.*, The SXS Collaboration catalog of binary black hole simulations, Classical Quantum Gravity **36**, 195006 (2019).
[83] M. A. Scheel *et al.*, The SXS Collaboration's third catalog of binary black hole simulations, Classical Quantum Gravity **42**, 195017 (2025).
[84] A. G. Abac *et al.* (LIGO Scientific Collaboration, KAGRA Collaboration, and VIRGO Collaboration), Observation of gravitational waves from the coalescence of a 2.5–4.5$M_\odot$ compact object and a neutron star, Astrophys. J. Lett. **970**, L34 (2024).
[85] P. Mahapatra, D. Chattopadhyay, A. Gupta, F. Antonini, M. Favata, B. S. Sathyaprakash, and K. G. Arun, Possible binary neutron star merger history of the primary of GW230529, Phys. Rev. D **111**, 123030 (2025).
[86] R. Abbott *et al.* (LIGO Scientific Collaboration and Virgo Collaboration), GWTC-2: Compact binary coalescences observed by LIGO and Virgo during the first half of the third observing run, Phys. Rev. X **11**, 021053 (2021).
[87] T. Dietrich, T. Hinderer, and A. Samajdar, Interpreting binary neutron star mergers: Describing the binary neutron star dynamics, modelling gravitational waveforms, and analyzing detections, Gen. Relativ. Gravit. **53**, 27 (2021).
[88] B. P. Abbott *et al.* (LIGO Scientific Collaboration and Virgo Collaboration), Tests of general relativity with GW150914, Phys. Rev. Lett. **116**, 221101 (2016); **121**, 129902(E) (2018).
[89] S. Husa, S. Khan, M. Hannam, M. Pürrer, F. Ohme, X. Jiménez Forteza, and A. Bohé, Frequency-domain gravitational waves from nonprecessing black-hole binaries. I. New numerical waveforms and anatomy of the signal, Phys. Rev. D **93**, 044006 (2016).
[90] M. Hannam, P. Schmidt, A. Bohé, L. Haegel, S. Husa, F. Ohme, G. Pratten, and M. Pürrer, Simple model of complete precessing black-hole-binary gravitational waveforms, Phys. Rev. Lett. **113**, 151101 (2014).
[91] T. Dietrich, A. Samajdar, S. Khan, N. K. Johnson-McDaniel, R. Dudi, and W. Tichy, Improving the NRTidal model for binary neutron star systems, Phys. Rev. D **100**, 044003 (2019).
[92] G. Ashton *et al.*, BILBY: A user-friendly Bayesian inference library for gravitational-wave astronomy, Astrophys. J. Suppl. Ser. **241**, 27 (2019).
[93] I. M. Romero-Shaw *et al.*, Bayesian inference for compact binary coalescences with BILBY: Validation and application to the first LIGO–Virgo gravitational-wave transient catalogue, Mon. Not. R. Astron. Soc. **499**, 3295 (2020).
[94] J. Buchner, A. Georgakakis, K. Nandra, L. Hsu, C. Rangel, M. Brightman, A. Merloni, M. Salvato, J. Donley, and D. Kocevski, X-ray spectral modelling of the AGN obscuring region in the CDFS: Bayesian model selection and catalogue, Astron. Astrophys. **564**, A125 (2014).
[95] M. Kesden, Can binary mergers produce maximally spinning black holes?, Phys. Rev. D **78**, 084030 (2008).
[96] D. A. Hemberger, G. Lovelace, T. J. Loredo, L. E. Kidder, M. A. Scheel, B. Szilágyi, N. W. Taylor, and S. A. Teukolsky, Final spin and radiated energy in numerical simulations of binary black holes with equal masses and equal, aligned or anti-aligned spins, Phys. Rev. D **88**, 064014 (2013).
[97] N. Andersson and K. Glampedakis, A Superradiance resonance cavity outside rapidly rotating black holes, Phys. Rev. Lett. **84**, 4537 (2000).
[98] W. Kastaun, F. Galeazzi, D. Alic, L. Rezzolla, and J. A. Font, Black hole from merging binary neutron stars: How fast can it spin?, Phys. Rev. D **88**, 021501 (2013).
[99] R. Dudi, T. Dietrich, A. Rashti, B. Bruegmann, J. Steinhoff, and W. Tichy, High-accuracy simulations of highly spinning binary neutron star systems, Phys. Rev. D **105**, 064050 (2022).
[100] S. D. Tootle, L. J. Papenfort, E. R. Most, and L. Rezzolla, Quasi-universal behavior of the threshold mass in unequal-mass, spinning binary neutron star mergers, Astrophys. J. Lett. **922**, L19 (2021).
[101] L. J. Papenfort, E. R. Most, S. Tootle, and L. Rezzolla, Impact of extreme spins and mass ratios on the post-merger observables of high-mass binary neutron stars, Mon. Not. R. Astron. Soc. **513**, 3646 (2022).
[102] S. Rosswog, P. Diener, F. Torsello, T. M. Tauris, and N. Sarin, Mergers of double NSs with one high-spin component: Brighter kilonovae and fallback accretion, weaker gravitational waves, Mon. Not. R. Astron. Soc. **530**, 2336 (2024).
[103] B. Karakas, R. Matur, and M. Ruffert, Effect of spin in binary neutron star mergers, arXiv:2405.13687.